A universal method based on fractional derivatives for modeling magnetic losses under alternating and rotational magnetization conditions

Benjamin Ducharne, S. Zurek, Gaël Sebald

A universal method based on fractional derivatives for modeling magnetic losses under alternating and rotational magnetization conditions

B. Ducharne[1,2], S. Zurek[3], G. Sebald[2]

1. LGEF, INSA Lyon, Villeurbanne, France.

2. ELyTMaX UMI 3757, CNRS – Université de Lyon – Tohoku University, International Joint Unit, Tohoku University, Sendai, Japan.

3. Megger Instruments, Archcliffe Road, Dover, CT17 9EN, United Kingdom

Abstract:

The performance of electromagnetic devices like motors and transformers is dictated by their efficiency of magnetic energy conversion, and the adequate modeling of this efficiency is essential in device design processes. However, a universal model that yields satisfactory results for this process under both alternating and rotating magnetic fields has yet to be developed. The present work addresses this issue by extending a previously proposed vector dry-friction modeling method to include frequency dependence using fractional derivative operators. The resulting vector model relies on eight parameters that can be adjusted to fit a wide range of experimental data, and thereby provides accurate estimations of magnetic losses over broad frequency bandwidths under both alternating and rotating magnetic fields. The model provides excellent agreement with the commonly observed reduction in magnetic losses when approaching saturation under low frequency rotating excitations, and further includes overshadowing with eddy current loss as the frequency increases. The accuracy and universality of the model are demonstrated under both alternating and rotational magnetization conditions based on comparisons with experimental results.

Keywords:

Magnetic hysteresis, simulation tool, fractional derivative, alternating losses, rotating losses, magnetic losses.

1 – Introduction

The performance of electromagnetic devices depends largely on their magnetic energy conversion efficiency. Progress in the understanding and modeling of magnetization responses has promoted the emergence of advanced magnetic circuits leading to continuous improvements in the magnetic energy conversion efficiencies of electromagnetic devices. Moreover, the ability to model magnetization responses accurately significantly reduces the conception times and the experimental effort required for developing high-performance electromagnetic devices. However, modeling methods must be capable of addressing a wide range of conditions in modern applications. For example, contemporary magnetic circuit designs, such as those found in power electronics, are exposed to high frequency and high amplitude magnetic excitations, which introduce harsher working conditions than exist for conventional applications operating at sinusoidal voltages. In addition, the motors in electrical vehicles operate under complex excitation waveforms at elevated frequencies due to the switch-mode power supplies employed for the smooth regulation of speed and power. Accordingly, efforts to support further performance improvements in the magnetic energy conversion efficiencies of electromagnetic devices must include highly advanced numerical methods that offer good agreement with real-life observations.

Efforts to develop new numerical methods for modeling the magnetization responses of electromagnetic devices must consider the practical objectives of this time-consuming development carefully. A good example of this issue pertains to the modeling of the magnetic hysteresis cycle. Here, the evolution of the magnetization state **M** of a system as a function of the surface tangent magnetic excitation $\mathbf{H_{surf}}$ is a classic example of magnetic behavior. The hysteresis cycle is typically measured following standard characterization practices based on well-defined experimental conditions [1]-[3]. However, the magnetization state **M** is not directly accessible in experiments, and it is replaced in practice by the averaged induction $\mathbf{B_a}$ obtained by integrating the electromotive force induced in a B-coil over time. In addition, $\mathbf{H_{surf}}$ is obtained through current measurements in conjunction with some assumptions. All standard characterizations assume that $\mathbf{B_a}$ and $\mathbf{H_{surf}}$ are collinear, and are replaced by their magnitudes B_a and H_{surf}, which leads to a $B_a(H_{surf})$ hysteresis cycle. In addition, most standard characterizations include compensation for the air flux component, which yields a value of $\mathbf{J_a}$ rather than $\mathbf{B_a}$, from which the magnetization state $\mathbf{M_a}$ can be obtained by scaling through the permeability of free space. We further note that magnetic hysteresis curves include the following magnetization responses:

- domain wall bulging in the low H_{surf} range [4];
- irreversible domain wall motion in the middle H_{surf} range [5];

- magnetization rotation in the high H_{surf} range [6];
- domain wall frequency dependence, ripple, and avalanche phenomena [7]-[9];
- macroscopic eddy currents [10].

Accordingly, magnetic hysteresis phenomena are formed from the complex superimposition and the interactions of these responses and are therefore very difficult to understand and model.

The first attempts at modeling magnetic hysteresis phenomena mathematically were proposed at the end of the 19th century. The objective was to predict the magnetic core losses of ferromagnetic materials as a function of both the magnitude and frequency of $\mathbf{H}_{\mathbf{surf}}$ [11]. This loss problem is of genuine interest because magnetic core losses impact the conversion efficiency and the temperature distribution of electromagnetic devices. Since this early effort, numerous studies have focused on the modeling of hysteresis phenomena and the quantification of magnetic losses [12]-[15]. The modeling of magnetic energy losses under alternating magnetization have been studied for many decades. However, well-known loss estimation methods, such as the Statistical Theory of Losses (STL) [12][16], that have been used for many years suffer from serious limitations in terms of the wide range of dynamic conditions encountered in modern electromagnetic applications. This has been addressed in recent years by the development of alternative methods for modeling magnetic energy losses based on mathematical operators derived from the framework of fractional derivatives [17][18]. Even

though fractional calculus was introduced more than two centuries ago, it has only very recently found application in real-life problems, such as in biology and finance [19]. Time fractional derivatives are particularly useful for long-time heavy tail decays, which implies that the totality of past states have an inherent effect on a time t derivative. Accordingly, time fractional derivatives are well suited to an analysis of ferromagnetic hysteresis phenomena because present behavior is strongly correlated with historical behavior.

These recent advances have greatly increased the sophistication of modeling a wide range of magnetic responses [20]-[24]. However, these efforts have been disproportionately restricted to alternating magnetic field conditions, while developments appropriate under rotating magnetic field conditions are relatively unreported. The two primary reasons for this can be given as follows:

- lack of experimental data, which is most probably due to the absence of appropriate characterization standards;
- the complexity of rotating magnetization conditions, which must be analyzed vectorially.

Despite numerous attempts [20][22]-[25], improvements can still be obtained in the development of a universal model that yields satisfactory results for the magnetic responses of electromagnetic devices under both alternating and rotating magnetic fields.

These issues would be partially addressed by the use of a quasi-static modeling method. In this regard, we note that the quasi-static hysteresis loss contribution W_{hy} observed in the low-frequency range is thought to be frequency independent due to the decoupling of domain wall motions from the dynamical behaviors of H_{surf}. A good estimation of W_{hy} can be obtained by assuming that domain wall motion occurs under mechanical dry-friction conditions [26]. In fact, this concept was first proposed previously by Bergqvist [27]. Furthermore, we note that the use of fractional derivatives provides great flexibility for modeling frequency dependencies. A number of related methods have obtained good results for the modeling of ferromagnetic losses under alternating magnetization, such as fractional differential equations [17][18] and fractional diffusion [28][29]. However, to the best of our knowledge, fractional derivatives have never been used for modeling ferromagnetic losses under rotating magnetization.

The present study applies a quasi-static modeling method based on a combination of the previously proposed dry-friction (DF) model and frequency-dependent contributions formulated as mathematical operators collected within a framework of fractional derivatives, and thereby develops a universal electromagnetic model applicable to a wide range of magnetization conditions. The DF model assumes that only thermodynamic metastable states give rise to the anhysteretic curve $M = M_{anh}(H_{surf})$, and the presence of potential wells generate sequences of small discontinuous jumps similar to what is observed under mechanical dry-friction conditions.

Under these conditions, the resulting magnetic behavior produces a well-defined hysteresis response as the number of discontinuous jumps approaches infinity. The DF model is first developed under a quasi-static scalar configuration, where $\mathbf{B_a}$ and $\mathbf{H_{surf}}$ are assumed to be collinear, and the model is then extended from quasi-static to high-frequency conditions. Issues regarding congruency and accommodation are discussed. Special attention is devoted to the frequency effect and the use of fractional derivative operators for estimating magnetic loss. While an assumption of collinearity between $\mathbf{B_a}$ and $\mathbf{H_{surf}}$ is an absolutely necessary condition for obtaining reliable, reproducible, and comparable experimental results, this practical limitation is unnatural because magnetic fields are vector quantities, and such collinearity is never evident in the real-life behavior of magnetic circuits. Therefore, a vector configuration of the DF model is developed for examining magnetic losses under rotating magnetization conditions. Finally, the accuracy and universality of the model are demonstrated under both alternating and rotational magnetization conditions based on comparisons with experimental results.

2 – Scalar dry-friction model

2.1 Quasi-static modeling method

The construction of the quasi-static DF model is based on a major $B_a(H_{surf})$ hysteresis cycle obtained by applying the following sequence of relationships between $H_{surf}(t)$ and $B_a(t)$ as a function of time t for a single DF element.

$$if\ H_{surf}(t) > f^{-1}(B_a(t-dt)) + H_c$$

$$B_a(t) = f(H_{surf}(t) - H_c)$$

$$if\ H_{surf}(t) < f^{-1}(B_a(t-dt)) - H_c$$

$$B_a(t) = f(H_{surf}(t) + H_c)$$

$$else\ B_a(t) = B_a(t-dt) \quad (1)$$

Here, H_c is the coercivity and $f(\cdot)$ is a sigmoid function related to the anhysteretic behavior, which is denoted as $B_{anh}(H_{surf})$, and is defined as follows:

$$B_{anh} = \frac{2}{\pi} B_s \tan^{-1}\left(\frac{H_{surf}}{a}\right), \quad (2)$$

where B_s and a are the anhysteretic function parameters.

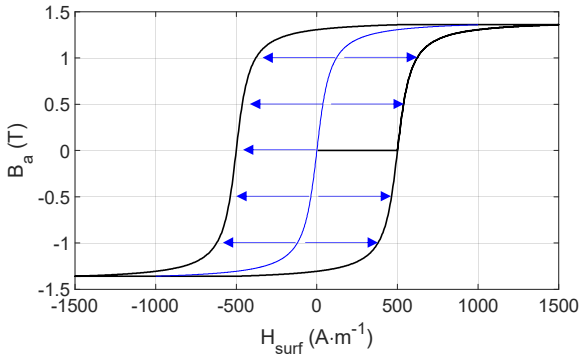

Fig. 1 Major hysteresis cycle obtained from the sequence given by Eq. (1).

Sequence (1) provides a good approximation of the main features of a major hysteresis cycle observed under steady-state conditions with symmetrical high-amplitude H_{surf} excitation. However, this sequence is incapable of modeling transient phases, such as the first magnetization curve and minor loops, although this restriction can be mitigated. For example, Ducharne et al.

[26] addressed this issue by replacing the single DF element with a system composed of *k* elements having different coercivity values and different weights characterizing their individual impacts on the overall hysteresis behavior. The distribution of the coercivity values of the elements was considered homogeneous with a constant ΔH_{surf} step, and their corresponding weights were defined according to the following spectrum function.

$$B_a = \sum_{i=1}^{k} Spectrum(H_{c_i}) B_{a_i} \quad (3)$$

Good results can be obtained by defining the spectrum function according to the following Gaussian function:

$$Spectrum(H_{c_i}) = \frac{e^{-\frac{(H_{c_i}-\mu)^2}{2\sigma^2}}}{\sigma\sqrt{2\pi}} \quad (4)$$

where μ is the Gaussian function average and σ is its standard deviation. The product $\mu \cdot \Delta H_{surf}$ is equal to the coercivity of the simulated hysteresis cycle $B_a(H_{surf})$. Similarly, σ is defined according to the ratio of the differential permeabilities of the simulated anhysteretic curve $B_{anh}(H_{surf})$ and at the coercivities of the simulated $B_a(H_{surf})$ curve. The use of a Gaussian function is particularly beneficial because it involves only two parameters μ and σ. These parameters can be set easily based on experimental data. However, a previous study adopted a numerical solution for defining the spectrum function by deconvolving the first magnetization curve by the anhysteretic curve [30]. While this solution produced very accurate results, the methodology requires the

anhysteretic curve, which is difficult to obtain experimentally, and the complexity of calculating the spectrum curve increases exponentially with an increasing number of DF elements because each DF element is characterized by its own parameter. In contrast, the use of a Gaussian function with only two parameters means that the number of DF elements in the DF model is not constrained. Finally, the distribution of the spectrum function must be normalized, such that

$$\sum_{i=1}^{k} Spectrum\left(H_{c_i}\right) = 1. \quad (5)$$

The first magnetization portion of the major $B_a(H_{surf})$ hysteresis loop obtained using the DF model and the Jiles-Atherton (JA) model for a typical laminated FeSi 3 wt% GO electrical steel sheet are presented in Fig. 2a. The parameters employed for both models are listed in Table 1, where the JA model parameters were those adopted in a previous study [31]. In addition, the spectrum function distribution employed for the DF model is given in Fig. 2b.

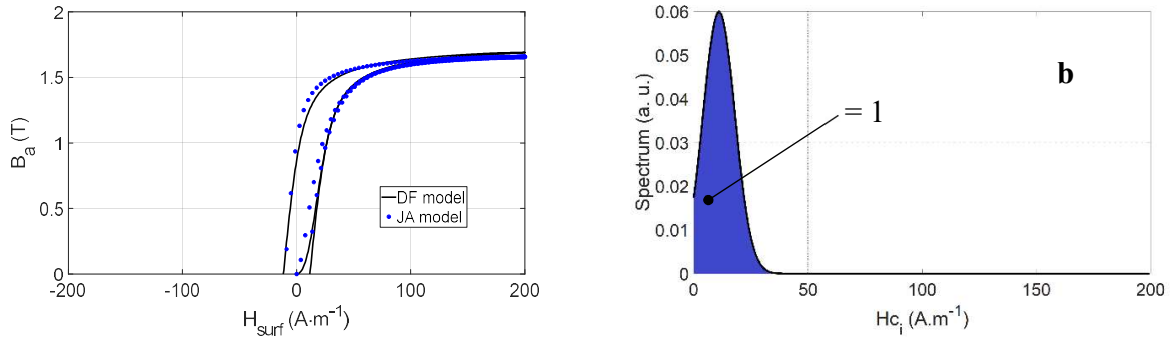

Fig. 2 a) Comparison of DF and JA model results for the first magnetization portion of the major hysteresis loop of laminated FeSi 3 wt% GO sheet steel. b) DF model spectrum function distribution.

Table 1 Parameter values employed by the JA and DF models to obtain the plots given in Figs. 2a and b.

JA model parameters	Typical value	DF model parameters	Typical value
a (A·m^{-1})	6	a (A·m^{-1})	10

M_s (A·m^{-1})	1353000	B_s (T)	1.7
k (A·m^{-1})	19	μ	12
c	0.15	σ	7
α	$8 \cdot 10^{-6}$	k	200

2.2 Congruency and the accommodation status

An essential limitation of the DF model in its standard form derives from the unique dependence of H_{surf} on the magnetization state **M**. This limitation is particularly problematic when the modeled condition corresponds to a minor loop bounded by two sets of H_{surf} values because the size and the shape of the resulting $B_a(H_{surf})$ prediction do not depend upon the magnetization state of the specimen. This phenomenon is denoted as the congruency property, which has been discussed in many publications [32][33]. This is an inherent property of most history-dependent modeling methods [33] and, more specifically, the well-known Preisach model [34].

Congruency issues are, of course, a problem if the model converges toward a prediction that is inconsistent with real-life observations. Still, aside from the purely academic challenge associated with this issue, the question of whether the occurrences of minor loops must be modeled accurately at all is legitimate. This question can be evaluated according to an investigation of the magnetic incremental permeability (MIP) signature, which is a relevant

indicator of residual stresses and strains in structural steel components and can thereby serve as a non-destructive testing (NDT) technique [35]-[38].

The MIP signature of a material is measured as the superimposition of a slowly varying, high amplitude $H_{surf_{DC}}$ contribution to a low amplitude, high frequency $H_{surf_{AC}}$ magnetic excitation, which yields a so-called "butterfly" loop associated with the evolution of the incremental permeability modulus $\left|\underline{\mu_{MIP}}\right|$ as a function of the $H_{surf_{DC}}$ magnetic excitation. These simultaneous magnetic excitations generate a major hysteresis cycle trajectory that is slightly augmented in shape and size due to a large number of minor, low-amplitude asymmetric loops. Congruent models are inept at modeling proper butterfly loops, and can only provide a unique curve when increasing and decreasing H_{surf} behaviors coincide.

The classic resolution of the congruency issue is to replace the model input H_{surf} by an effective excitation field H_e, where the magnetization state is considered according to an adjustable parameter α as follows.

$$H_e = H_{surf} + \alpha \cdot B_a. \tag{6}$$

The DF model is accordingly extended by replacing H_{surf} with H_e. In addition, Eq. (4) is still used for the spectrum function. However, the method employed for estimating the parameters μ and σ previously is no longer appropriate, and is replaced by a numerical method involving the minimization of the mean relative standard deviation error function in comparison with

experimentally measured values. For modeling $\left|\underline{\mu_{MIP}}\right|$ as a function of $H_{surf_{DC}}$, the error function is given as follows:

$$Error\ (\%) = \frac{100}{q}\sum_{i=1}^{q}\frac{\left||\mu_{rMIP}|_{i_{meas}}(H_i)-|\mu_{rMIP}|_{i_{sim}}(H_i)\right|}{|\mu_{rMIP}|_{i_{meas}}(H_i)}, \quad (7)$$

where the subscripts *meas* and *sim* respectively represent the *q* discrete data points obtained experimentally and those obtained from the extended DF model. For a standard $B_a(H_{surf})$ curve like that given in Fig. 2a, the error function is given as follows.

$$Error\ (\%) = \frac{100}{q}\sum_{i=1}^{q}\frac{\left|B_{i_{meas}}(H_i)-B_{i_{sim}}(H_i)\right|}{B_{i_{meas}}(H_i)} \quad (8)$$

In both cases, the error function is calculated on the portion of the curve obtained under increasing H_{surf}.

An illustration of the congruency correction obtained using Eq. (6) is presented in Fig. 3a, where minor loops are obtained by the DF model using H_e for a given H_{surf} window and different initial magnetization states. Here, Eq. (4) is still used for the spectrum function, and the parameters of the extended DF model are presented in Table 2. A comparison of modeling and experimental results reflecting the butterfly loop associated with the value of $\left|\underline{\mu_{IP}}\right|$ as a function of $H_{surf_{DC}}$ is presented in Fig. 3b for laminated FeSi 3 wt% GO electrical steel sheet. The experimental results were obtained with a previously described experimental setup [39][40]. The results of the DF model in Fig. 3b were obtained by locally modifying the parameters of the DF element characterized by the absence of coercivity ($Hc_1 = 0$), where the parameters

$Spectrum_{Hc}$, a_{Hc} , and Bs_{Hc1} in Table 2 correspond to the modified weight and anhysteretic parameters of this element. Finally, the results presented in Fig. 2a are repeated here for the extended DF model in Fig. 3c and very minor differences are observed.

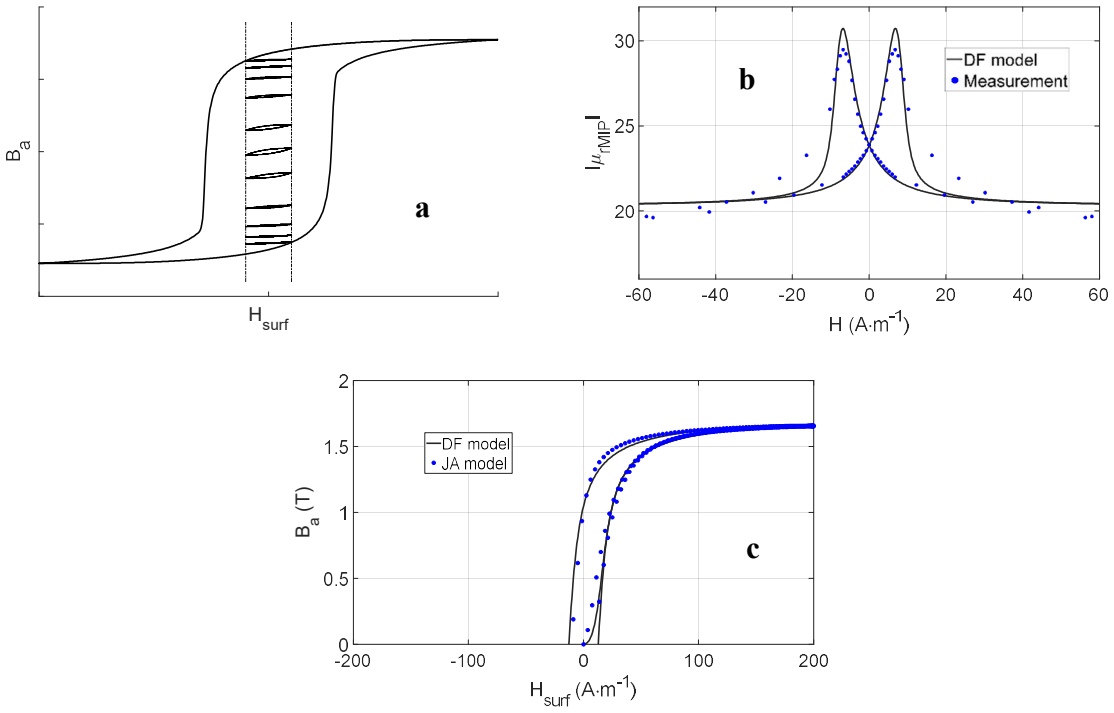

Fig. 3 a) Illustration of congruency correction, where minor loops are obtained by the DF model using H_e in Eq. (6) for a given H_{surf} window and different initial magnetization states. b) Comparison of modeling and experimental results reflecting the butterfly loop associated with the magnetic incremental permeability (for additional information about the experimental setup, see [39][40]). c) Comparison of DF and JA model results for the first magnetization portion of the major hysteresis loop of laminated FeSi 3 wt% GO sheet steel after consideration of the effective excitation field based on Eq. (6).

Table 2 DF model parameters employed for the results given in Fig. 3.

DF model parameters	Typical value
a (A·m^{-1})	10
B_s (T)	1.7
μ	12
σ	8

k	200
α	8

First element (Hc_1 = 0) parameters	**Typical value**
$Spectrum_{Hc1}$ (a. u.)	0.0003
a_{Hc1} (A·m^{-1})	14
Bs_{Hc1} (T)	1.7

Like congruency, accommodation is a ferromagnetic hysteresis phenomenon that can be observed within minor loops cycled at some rate between two magnetic fields, where the loop extremities undergo small shifts at each cycle that are independent of the cycling rate [35]. In experimental observations, these shifts depend upon the nature of the material, the width of the minor loops, and their locations within the major hysteresis envelope. Accommodation is a complex and elusive phenomenon that often presents itself as a transient modification of minor hysteresis loops, which disappears after some number of cycles. While methods have been proposed for modeling this phenomenon, the resulting models have been rarely validated based on experimental data [41][42]. Past studies have demonstrated that increasing the $H_{surf_{DC}}$ contribution incrementally during MIP signature measurements while monitoring the eddy current testing (ECT) coil impedance used for implementing the $H_{surf_{AC}}$ contribution is a good indirect means of observing the accommodation phenomenon [43]. However, the extension of the DF model to account for accommodation phenomena is not explicitly treated in the present

study owing to space restrictions. Nonetheless, replacing H_{surf} by H_e solved the congruency issue, but also generated some accommodation effects, and thus is potentially a solution for addressing the accommodation simulation.

2.3 Extension of the scalar model for alternating magnetization and frequency dependency

2.3.1 Fractional derivative operators

Among the multiple definitions of time-fractional derivatives found in the literature, the following forward Grünwald-Letnikov is very commonly employed [44].

$$\begin{cases} D_f^n f(t) = \lim\limits_{h\to 0^+} h^{-n} \sum_{m=0}^{\infty} \frac{(-n)m}{m!} f(t-mh) \\ (n)_m = \frac{\Gamma(n+m)}{\Gamma(n)} = m(m+1)\dots(n+m-1) \\ (m)_0 = 1 \end{cases} \tag{9}$$

Here, $(n)_m$ is known as the Pochhammer symbol and Γ is the gamma function. In the present context, h represents a time step, n represents the fractional order, and $f(\cdot)$ is a given analytical function. The following Riemann-Liouville form is also commonly employed [45].

$$D_f^n f(t) = \frac{1}{\Gamma(1-n)} \frac{d}{dt} \int_{-\infty}^{t} (t-\tau)^{-n} f(\tau) d\tau \tag{10}$$

2.3.2 Magnetic energy loss modeling using fractional derivative operators

As discussed, alternative methods have been developed based on fractional derivative operators for modeling magnetic energy losses. Among these different approaches include that based on the following fractional differential equation [17][18]:

$$\rho \frac{d^n B_a}{dt^n} = H_{surf}(t) - H_{stat}(B_a), \tag{11}$$

where ρ is a constant and H_{stat} is a fictitious coercivity value calculated from a quasi-static model of a specific material. In addition, hybrid solutions have been developed, such as by partially modifying the STL method via the introduction of fractional derivative operators for modeling eddy current losses under both low and high frequencies [46]. Assuming that the skin effect affects only the classical eddy current loss W_{cl}, the usual expression of magnetic loss W can be replaced by the following expression based on fractional derivatives.

$$W = W_{hy} + W_{cl} + W_{ex} = \oint_l \left[H_{surf}(B_a(t))\right] dB_a \tag{12}$$

Here, W_{hy} is the hysteresis loss, W_{ex} is the excess eddy current loss, and H_{surf} has been defined as

$$H_{surf} = H_{hy} + H_{cl} + H_{ex}, \tag{13}$$

where H_{hy}, H_{cl}, and H_{ex} are the hysteresis, the eddy current, and the excess magnetic field contributions, respectively. This yields the following expressions.

$$W = \oint_l \left[H_{hy}\big(B_a(t)\big) + H_{cl}\big(B_a(t)\big) + H_{ex}\big(B_a(t)\big)\right] dB_a \tag{14}$$

$$W = \oint_l \left[H_{hy}\big(B_a(t)\big) + \rho \frac{d^n B_a(t)}{dt^n} + \sqrt{\vartheta S G V_0} \left|\frac{dB_a}{dt}\right|^{0.5}\right] dB_a \tag{15}$$

Here, ϑ is the electrical conductivity, *S* is the cross-sectional area, *G* is a dimensionless coefficient, and V_0 is a statistical parameter related to the distribution of local coercive fields, which collectively represents the role of microstructure [16]. Finally, the following anomalous fractional diffusion equation is another option that has been demonstrated to provide satisfactory results over a significant range of frequencies [28][29].

$$\nabla^2 H_{surf} = \vartheta \frac{d^n B_a}{dt^n} \tag{16}$$

All of these methods can be applied to the quasi-static DF model proposed herein. However, only the fractional differential equation (11) will be applied in the following discussion owing to space restrictions. Detailed descriptions of these other methods can be found elsewhere [28][29].

2.3.3 Application of the fractional differential equation for incorporating frequency dependence in the dry-friction model under alternating magnetization

The characteristics of domain-wall motions change at higher frequencies when the quasi-static condition is not satisfied, and additional losses must be considered. This issue can be addressed in the DF model by combining DF elements with viscoelastic elements as follows.

$$if\ H_{surf}(t) > f^{-1}\left(B_a(t-dt) + \rho \cdot \frac{d^n B_a(t-dt)}{dt^n}\right) + H_c$$

$$B_a(t) = f(H_{surf}(t) - \rho \cdot \frac{d^n B_a(t-dt)}{dt^n} - H_c)$$

$$if\ H_{surf}(t) < f^{-1}\left(B_a(t-dt) + \rho \cdot \frac{d^n B_a(t-dt)}{dt^n}\right) - H_c$$

$$B_a(t) = f(H_{surf}(t) - \rho \cdot \frac{d^n B_a(t-dt)}{dt^n} + H_c)$$

$$else\ B_a(t) = B_a(t - dt) \tag{17}$$

Here, ρ, like n, can be adjusted individually for each DF element.

On the one hand, this approach seems in good agreement with the physics of ferromagnetism, and this is even more true when considering the additional losses due to magnetic diffusion separately (i.e., macroscopic eddy currents [8]). On the other hand, working under sinusoidal B_a imposed conditions offer a much simpler approach. Solving Eq. 11 under these conditions means that both the $\rho \cdot \frac{d^n B_a}{dt^n}$ and $H_{stat}(B_a)$ terms can be calculated separately. The quasi-static term can be obtained explicitly using an *H*-imposed model and, for each simulation step time t, testing a window of H_{surf} centered around its value at $t = t - dt$. Fig. 4c presents an illustration of the resulting $H_{surf}(t)$ curve.

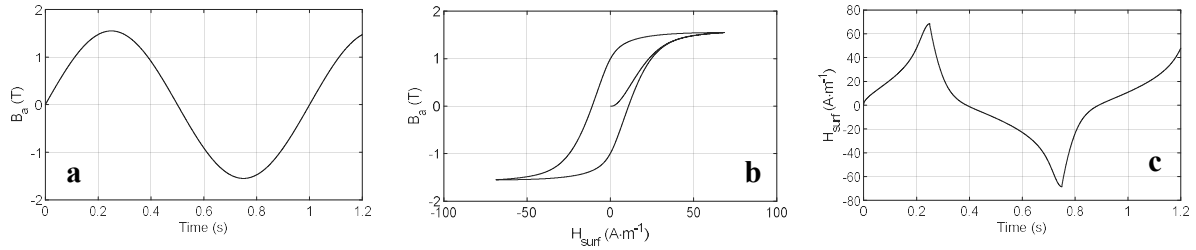

Fig. 4 a) Imposed sinusoidal $B_a(t)$ signal with a magnitude of 1.5 T and frequency of 1 Hz. b) Quasi-static hysteresis loop under imposed sinusoidal $B_a(t)$ conditions. c) Related $H_{surf}(t)$ obtained by the inverse DF model.

Finally, the magnetic losses obtained under alternating magnetic field conditions over a time period *T* are calculated as follows.

$$W_{alt} = \int_0^T \left(\frac{dB_a(t)}{dt} H_{surf}(t) \right) dt \tag{18}$$

The W_{alt} values obtained using the extended DF model with the dynamical parameters listed in Table 3 and various magnitudes $B_a(t)$ are compared with those obtained experimentally in Fig. 5 as a function of frequency under alternating magnetic excitation in the rolling direction (RD). The experimental results reported here derive from an earlier report associated with FeSi 3 wt% laminated GO electrical steel samples having a thickness d = 0.219 mm and a conductivity ϑ = 1.99×10^6 S·m^{-1} [46]. The errors associated with the modeled W_{alt} results were calculated using the following equation:

$$Error\ (\%) = \frac{100}{q} \sum_{i=1}^{q} \frac{\left| W_{meas_i} - W_{sim_i} \right|}{W_{meas_i}} \tag{19}$$

The obtained error values are listed in Table 4. We note that the error values range from about 4% to 20%, and that the average error obtained over all frequencies and magnitudes $B_a(t)$ was just 9.77%.

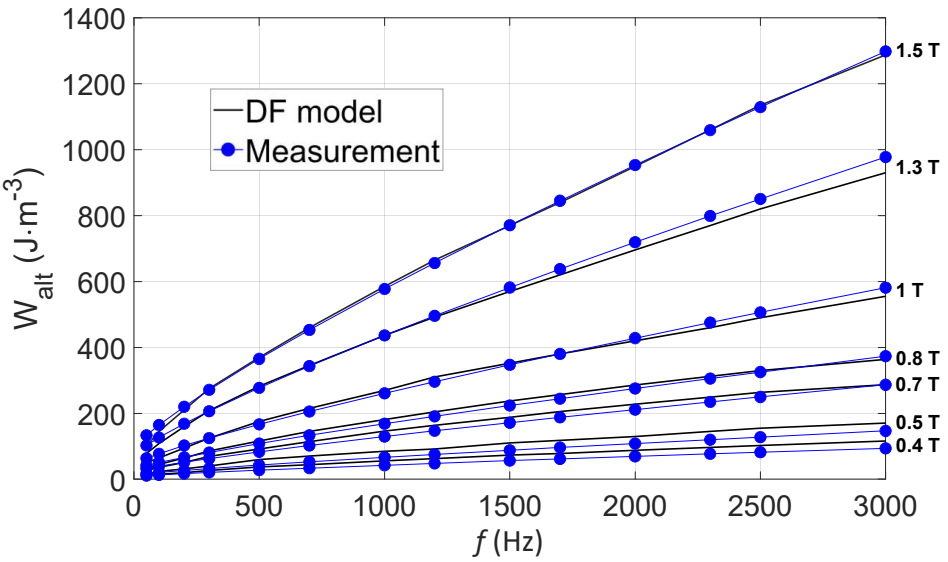

Fig. 5 Comparisons of magnetic losses W_{alt} obtained under an alternating magnetic excitation in the rolling direction via the dynamic DF model and corresponding experimental measurements.

Table 3 Dynamical DF model parameters.

Dynamical DF model parameters	Typical value
ρ	0.05
n	0.83

Table 4 Errors calculated by Eq. (19) for the W_{alt} results presented in Fig. 5.

Freq (Hz) / B_{MAX} (T)	50	100	200	300	500	700	1000	1200	1500	1700	2000	2300	2500	3000	Error (%)
0.4	0.67	10.12	13.68	22.64	26.45	23.13	23.16	23.37	22.70	21.39	21.10	20.66	20.11	19.03	19.16
0.5	7.64	13.73	15.96	18.61	28.31	24.62	21.70	18.10	19.92	18.36	16.61	17.12	17.50	13.72	17.99
0.7	21.61	10.17	1.55	8.86	9.36	10.08	11.28	10.24	8.66	8.34	7.21	5.78	5.42	0.15	8.48
0.8	24.01	12.25	2.96	4.78	6.73	8.17	7.19	6.62	5.86	4.79	3.81	2.17	1.39	2.63	6.67
1	27.33	19.37	7.74	0.00	4.66	4.26	3.33	4.46	1.39	0.03	2.00	3.36	3.32	4.77	6.14
1.3	31.85	17.02	5.14	0.73	1.70	0.54	0.15	0.77	2.08	2.84	3.34	3.74	3.76	5.16	5.63
1.5	33.13	13.43	4.85	1.41	1.28	1.51	1.34	1.31	0.12	0.61	0.40	0.03	0.53	0.79	4.34
Error (%)	20.89	13.73	7.41	8.15	11.21	10.33	9.74	9.27	8.68	8.05	7.78	7.55	7.43	6.61	9.77

3 – Vector dry-friction model

3.1 Quasi-static vector magnetic hysteresis model

The vector extension of the quasi-static DF model introduced in Subsection 2.1 has been introduced briefly in a previous report [27]. This extension is based on the following proposed modification of the sequence given in Eq. (20).

$$if \left|\overrightarrow{H_{surf}(t)} - \overrightarrow{f^{-1}(B_a(t-dt))}\right| \geq H_c$$

$$\vec{v} = \frac{\overrightarrow{H_{surf}(t)} - \overrightarrow{f^{-1}(B_a(t-dt))}}{\left|\overrightarrow{H_{surf}(t)} - \overrightarrow{f^{-1}(B_a(t-dt))}\right|}$$

$$H_c = \left|\overrightarrow{H_{surf}(t)} - \overrightarrow{f^{-1}\big(B_a(t-dt)\big)} - A\vec{v}\right|$$

$$\overrightarrow{B_a(t)} = f\left(\overrightarrow{f^{-1}\big(B_a(t-dt)\big)} + A\vec{v}\right)$$

$$else\ \overrightarrow{B_a(t)} = \overrightarrow{B_a(t-dt)} \tag{20}$$

Here, *A* is a constant and $\vec{v}$ is a unit vector giving the direction of change [27]. Their values are calculated at each discrete interval of time during the modeling process. In addition, the proposed vector extension introduces $\overrightarrow{f^{-1}\big(B_a(t-dt)\big)} + A\vec{v}$ as a rest field, which represents the field that would produce the observed magnetization state in the absence of hysteresis. This vector form of the DF model can readily accommodate anisotropic conditions by adjusting the directional dependences of the anhysteretic function parameters $a(\theta, \varphi)$ and $B_s(\theta, \varphi)$, where θ is the polar angle and φ is the azimuthal angle. However, no further details are given herein regarding the consideration of anisotropy due to space restrictions. This issue will be addressed in detail in an upcoming manuscript.

The viability of the proposed vector extension can be determined by evaluating the **B** dependence of the quasi-static losses W_{rot} obtained under a low-frequency rotational magnetization, where W_{rot} is calculated as follows.

$$W_{rot} = \int_0^T \left(\frac{dB_{ax}(t)}{dt} H_{surfx}(t) + \frac{dB_{ay}(t)}{dt} H_{surfy}(t) \right) dt \quad (21)$$

Here, B_{ax}, B_{ay}, H_{surfx}, and H_{surfy} are the projections of B_a and H_{surf} along the *x* and *y* axes, respectively. These results are presented in Fig. 6 for different maximal magnetic field magnitudes B_{aMAX}, f = 1 Hz, and the parameters listed in Tables 1 and 3. The results in the figure provide physically correct behavior in the low induction range. However, W_{rot} incorrectly continues increasing once the saturation elbow at approximately 1 T is reached. Indeed, W_{rot} is known from experimental observations to decrease in the high induction range following the disappearance of magnetic domains. Here, fewer domains mean fewer domain wall motions and fewer losses associated with them. Accordingly, the current form of the vector DF model is incapable of reproducing this decrease in W_{rot} in the high induction range.

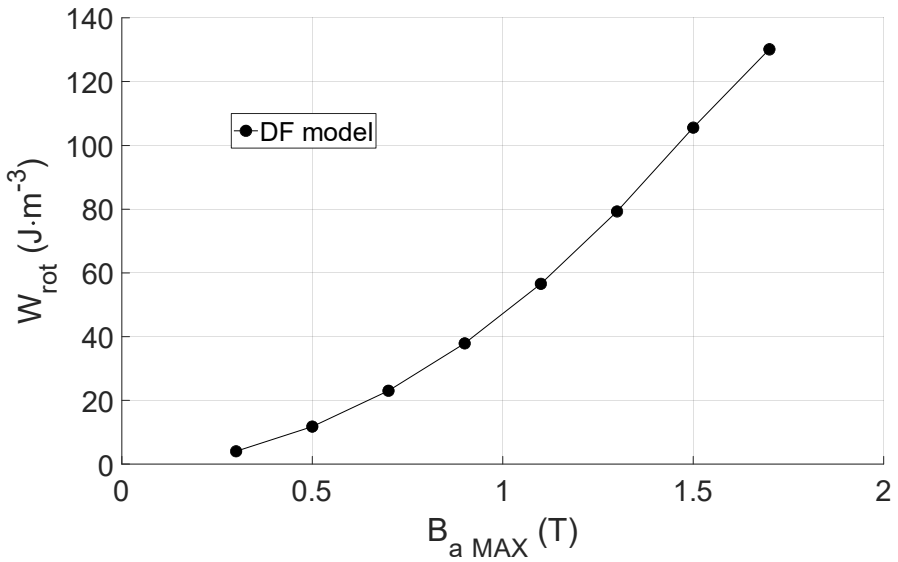

Fig. 6 Magnetic losses obtained from Eq. (21) for the vector configuration of the DF model (Eq. (20)) under rotational magnetization as a function of the maximal magnetic field amplitude B_{aMAX}.

This is a well-known issue that was addressed by Bergqvist [27] by conserving the spectrum function parameters and replacing the constant ΔH_{ci} step between the coercivity values of the DF elements with the following rest-field-dependent distribution function.

$$H_{c_i} = \frac{H_{c_{i_0}}}{\left(1+\left(\frac{\left|\overrightarrow{f^{-1}(B_a(t-d\ ))}+A\vec{v}\right|}{k_d}\right)^2\right)} \tag{22}$$

Here, k_d is an additional parameter that can be adjusted to fit the DF model to experimental results. This parameter is particularly helpful for adjusting the rotational losses obtained by the vector DF model because k_d has relatively little influence on the evolution of the magnetic losses W_{alt} obtained under alternating magnetic field conditions. The W_{rot} versus B_{aMAX} results originally presented in Fig. 6 are replicated in Fig. 7a based on the modification given in Eq. (22) with

different values of k_d. We note that the vector DF model now obtains physically correct behavior. Meanwhile, we plot the corresponding W_{alt} versus B_{aMAX} results in Fig. 7b, which clearly demonstrate that the proposed modification has little effect on W_{alt}. Finally, the modeled unidirectional hysteresis curves obtained with and without the proposed modification (k_d = 35) are presented in Fig. 7c. This figure confirms that the proposed modification has only a slight impact on the characteristics of the obtained hysteresis curve.

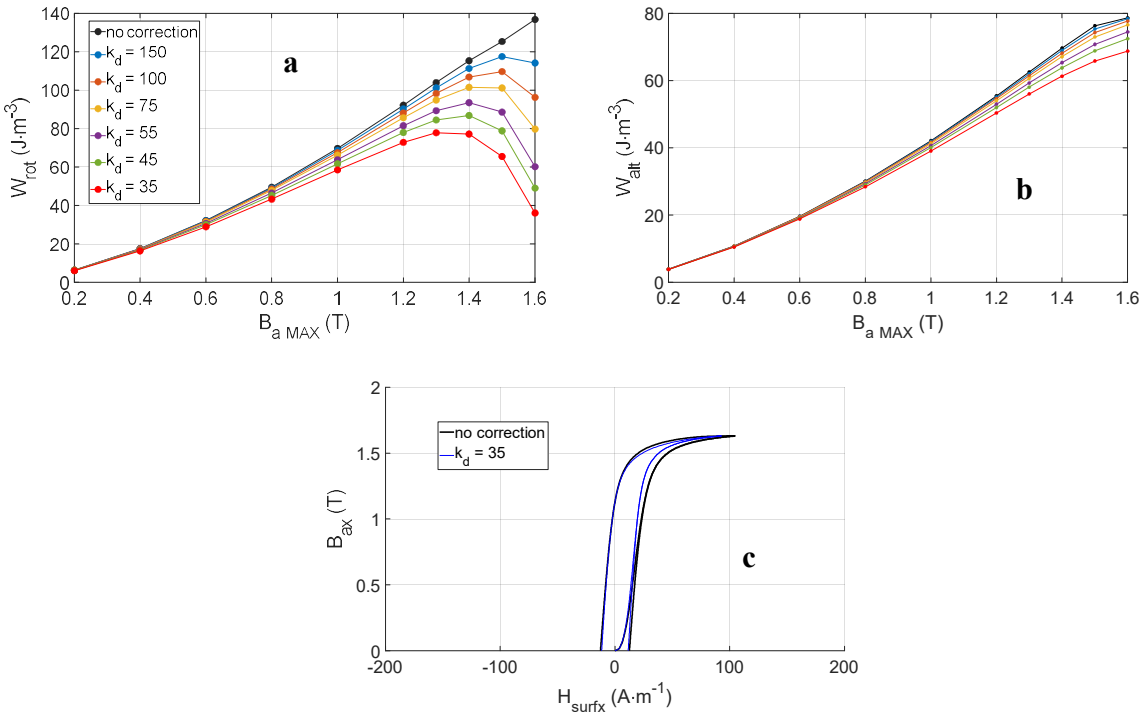

Fig. 7 a) Plot of W_{rot} as a function of B_{aMAX} without and with the proposed modification in Eq. (22) for different values of k_d. b) Plot of W_{alt} as a function of B_{aMAX} under equivalent conditions. c) Corresponding unidirectional hysteresis curve obtained with and without the proposed modification (k_d = 35).

3.1 Rotational magnetization and frequency dependency of the vector model

Under circular rotating B_a conditions, both B_{ax} and B_{ay} exhibit harmonic sinusoidal behaviors that are amendable to analytical solutions based on fractional derivatives. As was conducted above for losses under alternating magnetization, both the quasi-static and the frequency-dependent loss contributions can be calculated separately for both axes, and then added subsequently to obtain the total rotating loss W_{rot}. These static and dynamic rotational losses are calculated separately as follows.

$$W_{rot_{static}} = \int_0^T \left(\frac{dB_{ax}(t)}{dt} H_{surfx_{static}}(t) + \frac{dB_{ay}(t)}{dt} H_{surfy_{static}}(t) \right) dt \tag{23}$$

$$W_{rot_{dynamic}} = \int_0^T \left(\frac{dB_{ax}(t)}{dt} H_{surfx_{dynamic}}(t) + \frac{dB_{ay}(t)}{dt} H_{surfy_{dynamic}}(t) \right) dt \tag{24}$$

These equations adopt the following definitions based on fractional derivatives.

$$H_{surfx_{dynamic}}(t) = \rho \frac{d^n B_{ax}(t)}{dt^n} \tag{25}$$

$$H_{surfy_{dynamic}}(t) = \rho \frac{d^n B_{ay}(t)}{dt^n} \tag{26}$$

Finally, W_{rot} is obtained as follows.

$$W_{rot} = W_{rot_{static}} + W_{rot_{dynamic}} \tag{27}$$

We plot the values of W_{rot} obtained as a function of the fractional order n and the excitation frequency f (B_{aMAX} = 1.5 T, ρ = 0.01), and as a function of n and ρ (B_{aMAX} = 1.5 T, f = 100 Hz) in Figs. 8a and b, respectively. Here, the static parameters are those listed in Table 2 and k_d = 35. We note from the figures that W_{rot} is relatively insensitive to both f and ρ at low values of n. Nonetheless,

the parameters provide significant scope for adjusting the results of the vector DF model to accommodate a wide range of experimental results.

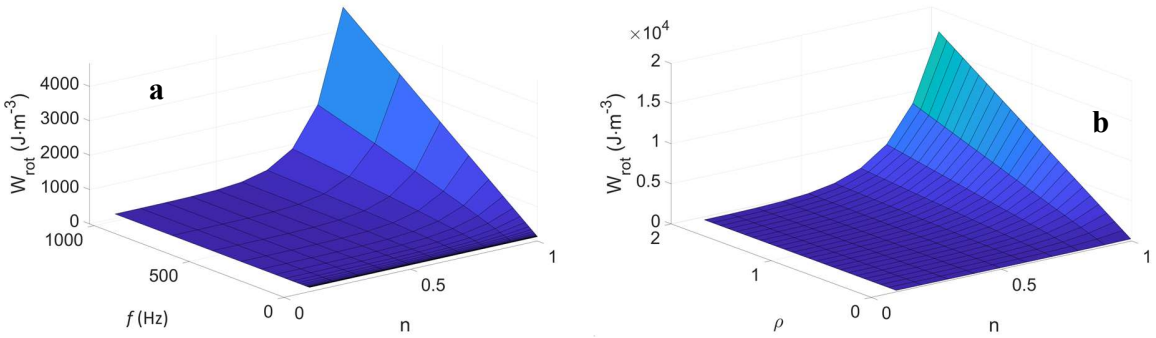

Fig. 8 Plots of W_{rot} obtained from Eq. (27) as functions of different model parameter values (B_{aMAX} = 1.5 T, k_d = 35, and all static parameters set according to Table 2): a) fractional order n and excitation frequency f (ρ = 0.01); b) n and ρ (f = 100 Hz).

The modeling capability of the proposed vector DF model was investigated by applying the parameter values listed in Tables 2 and 3 with k_d = 35, and comparing the plots of W_{rot} versus B_{aMAX} obtained by the model for various values of f with corresponding experimental results obtained for FeSi 3 wt% laminated GO electrical steel [47][48]. However, the experimental results are problematic because the grade of the test material is unknown. Moreover, only the rotational power loss was provided, and the related energy loss W was obtained from the following equation:

$$W = \frac{P \cdot \delta}{f}, \tag{28}$$

where P is the instantaneous power loss and δ = 7650 kg·m^{-3} is the density. These issues make efforts to validate the proposed universal model difficult because experimental results can be

obtained for magnetic losses under either alternating magnetization conditions or rotational magnetization conditions, but not both.

The modeling and experimental results are presented in Figs. 9a and b, respectively. In addition, these two data sources were plotted together in Fig. 9c to enable easy comparison. The results indicate that the modeling results are uniformly less than the experimental results by a factor of around 0.29. Nonetheless, a comparison of Figs. 9a and b demonstrate that the modeled behavior is quite close to the experimentally observed behavior qualitatively, despite the fact that the dynamic parameters in Table 3 were based on the magnetic loss data obtained under alternating magnetization conditions [46].

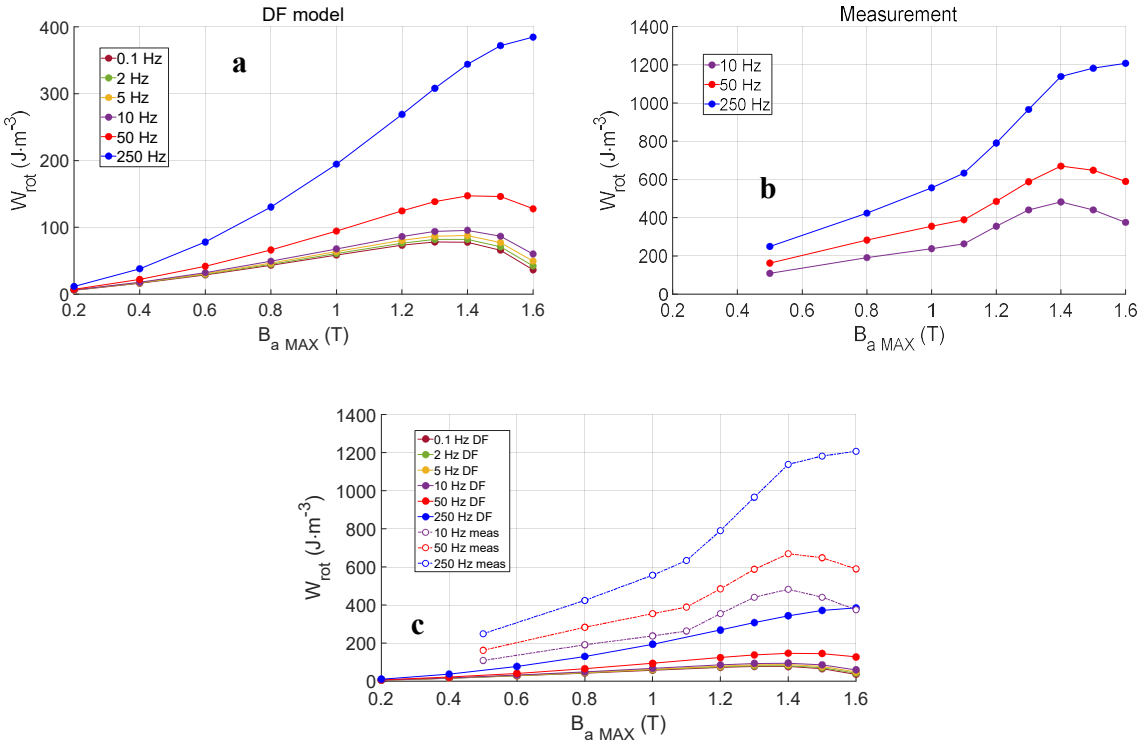

Fig. 9 Plots of W_{rot} versus B_{aMAX}: a) obtained from Eq. (27) for three values of f (k_d = 35 and all static and dynamic parameters set according to Tables 2 and 3, respectively); b) corresponding experimental values for FeSi 3 wt% laminated GO electrical steel [47]; c) plots in a) and b) given together for ease of comparison.

The modeling capability of the proposed vector DF model was investigated by applying the static parameter values listed in Table 2 and the modified dynamic parameters listed in Table 5 with k_d = 35, and comparing the plots of W_{rot} versus B_{aMAX} obtained by the model for various values of f with corresponding experimental results obtained for FeSi 3 wt% laminated GO electrical steel [47][48]. Here, the dynamic DF parameters listed in Table 5 were obtained by minimizing the following error function based on the differences between the experimental W_{rot} data points and the corresponding values obtained by the vector DF model.

$$Error\ (\%) = \frac{100}{q}\sum_{i=1}^{q}\frac{\left|W_{rot_{i_{meas}}}(B_i) - W_{rot_{i_{sim}}}(B_i)\right|}{W_{rot_{i_{meas}}}(B_i)} \tag{29}$$

The optimized dynamic parameters in Table 5 result in an error value of approximately 2.41%, which is clearly reflected by the very closely fitting results in Fig. 10.

Table 5 Dynamic DF model parameters employed for the rotational magnetization results in Fig. 10.

Dynamical DF model parameters	**Typical value**
ρ	0.0308
n	0.845

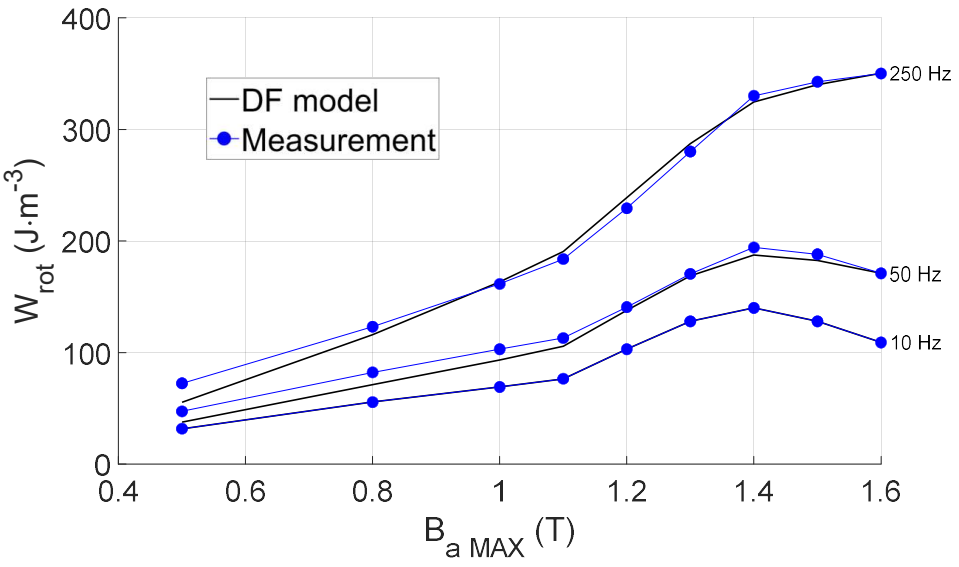

Fig. 10 Plots of W_{rot} versus B_{aMAX} obtained from Eq. (27) for three values of f (k_d = 35 and all static and dynamic parameters set according to Tables 2 and 5, respectively) and corresponding experimental values obtained for FeSi 3 wt% laminated GO electrical steel [49].

Finally, we present the experimentally observed $B_{ax}(H_{surfx})$ curves in the RD and the $B_{ay}(H_{surfy})$ curves in the transverse direction (TD) at the top of Fig. 11, and compare those with the corresponding curves obtained by the optimized vector DF model at the bottom of Fig. 11. The agreement between the curves was evaluated based on the maximum field error, which was calculated as follows.

$$max.\,field\ err._{\max(B_a)}\,(\%) = 100 \cdot \left(\frac{\left| \max\left(H_{surf_{meas}}\right) - \max\left(H_{surf_{sim}}\right) \right|}{\max\left(H_{surf_{meas}}\right)} \right) \qquad (30)$$

The error value obtained for the RD results was 7.4% and that for the TD results was 5.1%.

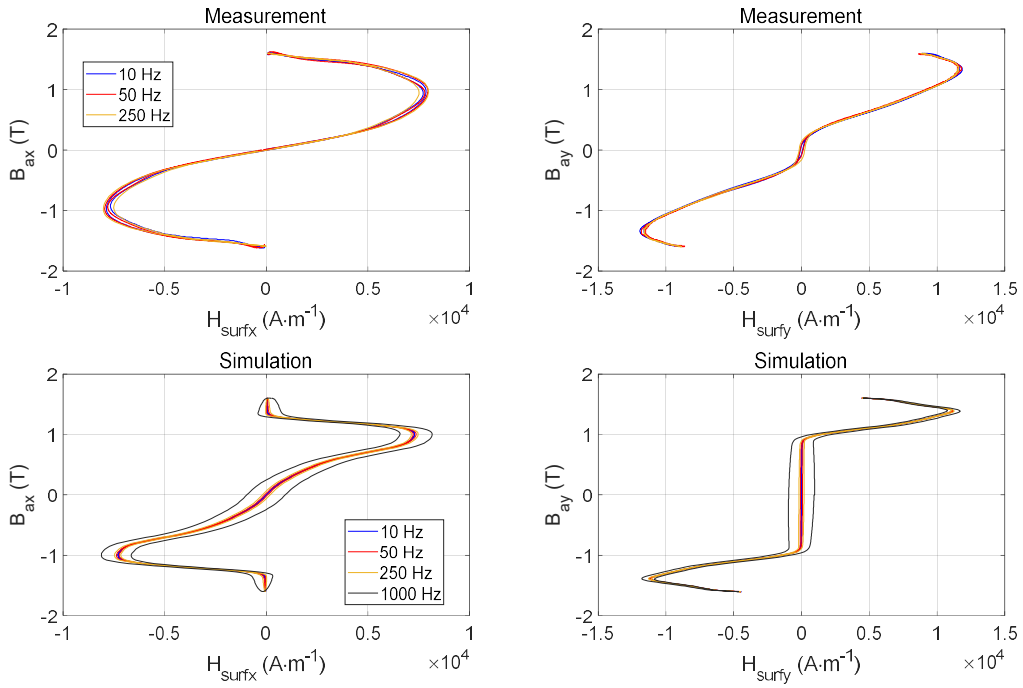

Fig. 11. Plots of B_{ax} versus H_{surfx} in the rolling direction (RD) and B_{ay} versus H_{surfy} in the transverse direction (TD) obtained experimentally for FeSi 3 wt% laminated GO electrical steel [49] and those obtained from the optimized vector DF model, which include results obtained at f = 1000 Hz for illustration purposes.

Recent studies focused on dynamic rotational magnetization conditions have introduced frequency dependence by applying a viscous loss consideration, where the dynamical contribution is given as the product of a constant and the first-order magnetization time derivative [49]-[52]. This study has opted for time-fractional derivatives, which are well suited to ferromagnetic hysteresis, and characterize real-time material behavior according to the fractional-order n. Here, $\mathrm{n} = 0$ represents a Hookean solid with characteristics pertaining to Hook's law, $\mathrm{n} = 1$ represents a Newtonian fluid, and viscoelastic behavior like that observed in

ferromagnetic materials occupy an intermediate range with $\mathrm{n} \in]0-1[$ [53]. Therefore, the use of fractional derivatives provides accurate modeling results over wide frequency bandwidths.

4 – Conclusion

In the present work, we tried to addressed the absence of a universal model that yields satisfactory modeling results for ferromagnetic materials under both alternating and rotating magnetic fields by applying a quasi-static modeling method based on a combination of a previously proposed DF model and frequency-dependent contributions formulated as mathematical operators within a fractional derivative framework. A quasi-static scalar DF model was first developed under the collinearity assumption. Issues regarding congruency and accommodation were discussed. Then, frequency dependence was introduced using fractional derivative operators. Finally, the DF model was developed within a vector configuration for modeling magnetic losses under rotating magnetization conditions.

A minimum of four experimental characteristics are required to an accurate description of a new material: a quasi-static high field unidirectional hysteresis cycle for the anhysteretic (M_s, γ) and hysteresis (μ, θ) parameters, a dynamic high field unidirectional hysteresis cycle for the dynamic parameters (ρ, n), a rotational high field projected

hysteresis cycle for the rotational losses parameter (k_d), an unsymmetrical behavior (first magnetization curve, minor loop, etc.) for the effective field parameter (α).

Comparisons of the results obtained by the DF model with experimental results for both alternating and rotational magnetization losses demonstrated that the eight parameters of the proposed DF model can be adjusted to fit a wide range of experimental data, and thereby provides accurate estimations of magnetic losses over broad frequency bandwidths under both alternating and rotating magnetic fields. However, the following two issues must be considered in future work.

- The DF model must be extended to account for accommodation phenomena explicitly.
- While a solution has been tentatively proposed for modeling anisotropic magnetic behaviors, this complex problem has yet to be outlined in detail.
- The modeling and experimental results were analyzed under the assumption that the external conditions, such as temperature and pressure, were both stable and reproducible. As a result, the influences of the these conditions on the magnetic responses of ferromagnetic materials have not been taken into consideration within the proposed DF model. Accordingly, these influences should be the object of future investigation.

References

[1] IEC 60404-2, “Magnetic materials – Part 2: Methods of measurement of the magnetic properties of electrical steel strip and sheet by means of an Epstein frame,” *International Electrotechnical Commission*, June 2008.

[2] IEC 60404-3, “Magnetic materials – Part 3: Methods of measurement of the magnetic properties of electrical steel strip and sheet by means of a single sheet tester,” *International Electrotechnical Commission*, April 2010.

[3] B. Koprivica, A. Milovanovic, M. Plazinic, “Standard methods of measurement of the magnetic properties of electrical steel stip an sheet,” *XI Int. SAUM conference on Systems, Automatic Control and Measurement*, Nis, Serbia, 2012.

[4] R. Valenzuela, I. Betancourt, “Giant magnetoimpedance, skin depth, and domain wall dynamics,” *IEEE Trans. Mag.*, vol. 38, iss. 5, pp. 3081 – 3083, 2002.

[5] F. Qiu, M.J. Klug, G. Tian, P. Hu, J. McCord, “Influence of magnetic domain wall orientation on Barkhausen noise and magneto-mechanical behavior in electrical steel,” *J. Phys. D: App. Phys.*, vol. 52, 265001, 2019.

[6] M. Carara, M. N. Baibich, R. L. Sommer, “Magnetization dynamics as derived from magneto impedance measurements,” *J. App. Phys.*, vol. 88, n°1, pp. 331 – 335, 2000.

[7] S.E. Zirka, Y.I. Moroz, P. Marketos, A.J. Moses, “Viscosity-based magnetodynamic model of soft magnetic materials,” *IEEE Trans. Mag.*, vol. 42, n°9, pp. 2121 – 2132, 2006.

[8] M.A. Raulet, B. Ducharne, J.P. Masson, and G. Bayada, “The magnetic field diffusion equation including dynamic hysteresis: a linear formulation of the problem,” *IEEE Trans. Mag.,* Vol. 40, n° 2, pp. 872-875, 2004.

[9] M. Petrun, S. Steentjes, “Iron-loss and magnetization dynamics in non-oriented electrical steel: 1-D Excitations up to high frequencies,” *IEEE Access*, vol. 8, pp. 4568-4593, 2020.

[10] C. Appino, O. de la Barrière, F. Fiorillo, M. LoBue, F. Mazaleyrat, C. Ragusa, “Classical eddy current losses in soft magnetic composites,” *J. App. Phys.*, vol. 113, 17A322, 2013.

[11] C.P. Steinmetz, “On the law of hysteresis,” AIEE Trans., vol. 9, pp. 3 – 64, 1892. Reprinted under the title “A Steinmetz contribution to the AC power revolution,” Introduction by J.E. Brittain, *Proc. IEEE*, vol. 72, n° 2, pp. 196 – 221, 1984.

[12] G. Bertotti, “General properties of power losses in soft ferromagnetic materials,” *IEEE Trans. Mag.*, vol. 24, n° 1, pp. 621 – 630, 1988.

[13] V. Malo Machado, A. Lopes Ribeiro, “Eddy current and hysteresis losses in ferromagnetic media,” *IEEE Trans. Mag.*, vol. 34, n° 4, pp. 1267-1269, 1998.

[14] S.E. Zirka, Y.I. Moroz, P. Marketos, A.J. Moses, D.C. Jiles, T. Matsuo, “Generalization of the classical method for calculating dynamic hysteresis loops in grain-oriented electrical steels,” *IEEE Trans. Mag.*, vol. 44, n° 9, pp. 2113 – 2125, 2008.

[15] B. Ducharne, G. Sebald, D. Guyomar, G. Litak, “Fractional model of magnetic field penetration into a toroidal soft ferromagnetic sample,” *Int. J. Dynam. Cont.*, **6,** 89–96 (2018).

[16] G. Bertotti, “Hysteresis in Magnetism,” San Diego, CA, USA: Academic, 1998.

[17] B. Zhang, B. Gupta, B. Ducharne, G. Sebald, T. Uchimoto, “Preisach’s model extended with dynamic fractional derivation contribution,” *IEEE Trans. Magn.*, Vol. 54, n° 3, pp. 1 – 4, 2018.

[18] B. Zhang, B. Gupta, B. Ducharne, G. Sebald, T. Uchimoto, “Dynamic magnetic scalar hysteresis lump model, based on Jiles-Atherton quasi-static hysteresis model extended with dynamic fractional derivative contribution,” *IEEE Trans. Magn.*, vol. 54, n° 11, pp. 1 – 4, 2018.

[19] S. Patnaik, J.P. Hollkamp, F. Semperlotti, “Applications of variable-order fractional operators: a review,” *Proc. R. Soc. A,* 476: 20190498, 2020.

[20] S. Ito, T. Mifune, T. Matsuo, C. Kaido, “Energy-Based Magnetization and Magnetostriction Modeling of Grain-Oriented Silicon Steel Under Vectorial Excitations,” *IEEE Trans. on Mag.*, vol. 52, n° 5, pp. 1 – 4, 2016.

[21] T. Matsuo, Y. Nishimura, Y. Mishima, T. Mifune, Y. Takahashi and K. Fujiwara, "Pinning Field Modeling Using Stop Hysterons for Multi-domain Particle Model," *2019 22nd International Conference on the Computation of Electromagnetic Fields (COMPUMAG)*, pp. 1 – 4, 2019.

[22] S. Steentjes, F. Henrotte, K. Hameyer, "Energy-based ferromagnetic material model with magnetic anisotropy," *J. Magn. Magn. Mater.,* vol. 425, pp. 20 – 24, 2017.

[23] K. Jacques, S. Steentjes, F. Henrotte, C. Geuzaine, K. Hameyer, "Representation of microstructural features and magnetic anisotropy of electrical steels in an energy-based vector hysteresis model," AIP Advances 8, 047602, 2018.

[24] X. Xiao, F. Müller, G. Bavendiek, K. Hameyer, "Analysis of vector hysteresis models in comparison to anhysteretic magnetization model," Eur. Phys. J. Appl. Phys. 91, 20901, 2020.

[25] E. Dlala, A. Belahcen, K.A. Fonteyn, M. Belkasim, "Improving loss properties of the Mayergoyz vector hysteresis model," *IEEE Trans. Mag.*, vol. 46, no. 3, pp. 918-924, 2010.

[26] B. Ducharne, D. Guyomar, G. Sebald, "Low frequency modelling of hysteresis behaviour and dielectric permittivity in ferroelectric ceramics under electric field," *J. Phys. D: App. Phys.*, Vol. 40, pp. 551-555, 2007.

[27] A. Bergqvist, "Magnetic vector hysteresis model with dry friction-like pinning," *Physica B: Cond. Matter*, vol. 233, Issue 4, pp. 342 – 347, 1997.

[28] B. Ducharne, Y.A. Tene Deffo, B. Zhang, G. Sebald, "Anomalous fractional diffusion equation for magnetic losses in a ferromagnetic lamination," *The Eur. Phys. J. Plus*, 135:325, 2020.

[29] B. Ducharne, P. Tsafack, Y.A. Tene Deffo, B. Zhang, G. Sebald, "Anomalous fractional magnetic field diffusion through the cross-section of a massive toroidal ferromagnetic core," *Com. in Nonlin. Sci. and Num. Sim.*, vol. 92, 105450, 2020.

[30] D. Guyomar, B. Ducharne, G. Sebald, "Time fractional derivatives for voltage creep in ferroelectric materials: theory and experiment," *J. Phys. D: App. Phys.*, Vol. 41, n° 12 125410, 2008.

[31] R.-A. Naghizadeh, B. Vahidi, S. H. Hosseinian, "Parameter identification of Jiles-Atherton model using SFLA," *COMPEL*, vol. 31, iss. 4, pp. 1293 – 1309, 2012.

[32] G. Kadar, E. Torre, “Hysteresis modeling: I. Non-congruency,” *IEEE Trans. Mag.*, vol. 23, no. 5, pp. 2820-2822, 1987.

[33] S. E. Zirka, Y. I. Moroz, P. Marketos, A. J. Moses, “Congruency-based hysteresis models for transient simulation,” *IEEE Trans. Mag.*, vol. 40, no. 2, pp. 390-399, 2004.

[34] I. D. Mayergoyz and G. Friedman, “Generalized Preisach model of hysteresis,” *IEEE Trans. Mag.*, vol. 24, no. 1, pp. 212-217, 1988.

[35] K. Li, L. Li, P. Wang, J. Liu, Y. Shi, Y. Zhen, S. Dong, “A fast and non-destructive method to evaluate yield strength of cold-rolled steel via incremental permeability,” *J. of Mag. and Mag. Mat.*, Vol. 498, 166087, 2020.

[36] A.N. Stashkov, E.A. Schapova, A.P. Nichipuruk, A.V. Korolev, “Magnetic incremental permeability as indicator of compression stress in low-carbon steel,” NDT & E Int., vol. 118, 102398, 2021.

[37] T. Matsumoto, T. Uchimoto, T. Takagi, G. Dobmann, B. Ducharne, S. Oozono, H. Yuya, “Investigation of electromagnetic nondestructive evaluation of residual strain in low carbon steels using the eddy current magnetic signature (EC-MS) method,” *J. of Mag. and Mag. Mat.*, Vol. 479, pp. 212 – 221, 2019.

[38] K. Li, Z. Zhang, P. Wang, Y. Liu, J. Zeng, “A novel 3D simulation prediction model of mechanical properties of ferromagnetic materials via incremental permeability method,” *J. of Mag. and Mag. Mat.*, Vol. 536, 168137, 2021.

[39] S. Zhang, B. Ducharne, S. Takeda, G. Sebald, T. Uchimoto, “Identification of the ferromagnetic hysteresis simulation parameters using classic non-destructive testing equipment,” *J. of Mag. and Mag. Mat.*, Vol. 531, 167971, 2021.

[40] B. Gupta, T. Uchimoto, B. Ducharne, G. Sebald, T. Miyazaki, T. Takagi, “Magnetic incremental permeability non-destructive evaluation of 12 Cr-Mo-W-V steel creep test samples with varied ageing levels and thermal treatments,” NDT & E International, vol. 104, pp. 42 – 50, 2019.

[41] B. Tellini, R. Giannetti, S. Lizon-Martinez, M. Marracci, “Characterization of the Accommodation Effect in Soft Hysteretic Materials Via Sensorless Measurement Technique,” *IEEE Trans. Inst. and Meas.*, vol. 58, n° 8, pp. 2807 – 2814, 2009.

[42] S. E. Zirka, Y. I. Moroz and E. Della Torre, “Combination hysteresis model for accommodation magnetization,” *IEEE Trans. Mag.*, vol. 41, no. 9, pp. 2426-2431, 2005.

[43] S. Zhang, B. Ducharne, S. Takeda, G. Sebald, T. Uchimoto, “Low frequency behavior of laminated electric steel sheet: investigation of ferromagnetic hysteresis loops and incremental permeability,” *J. of Mag. and Mag. Mat.*, vol. *538*, 168278, 2021.

[44] MD. Ortigueira, “Fractional calculus for scientists and engineers,” lecture notes in Electrical Engineering, 84, Springer, Dordrecht, 2011.

[45] MD. Ortigueira, M. Rivero, J.J. Trujillo, “From a generalised Helmholtz decomposition theorem to fractional Maxwell equations,” Commun. Nonlinear Sci. Numer. Simulat., vol. 22, pp. 1036 – 1049, 2015.

[46] R. Liu, L. Li, “Analytical prediction of energy losses in soft magnetic materials over broadband frequency range,” *IEEE Trans. Power Electron.,* vol. 36, n° 2, pp. 2009 – 2017, 2021.

[47] S. Zurek, “Characterisation of Soft Magnetic Materials Under Rotational Magnetisation”, Boca Raton, FL, USA:CRC Press, 2018.

[48] S. Zurek, T. Meydan, “Rotational power losses and vector loci under controlled high flux density and magnetic field in electrical steel sheets,” IEEE Transactions on Magnetics, Vol. 42, No 10, 2006, p. 2815-2817.

[49] T. Matsuo, M. Miyamoto, “Dynamic and Anisotropic Vector Hysteresis Model Based on Isotropic Vector Play Model for Non-Oriented Silicon Steel Sheet,” *IEEE Trans. Mag.*, vol. 48, n° 2, pp. 215 – 218, 2012.

[50] L. Zhu, J. Park and C. Koh, “A Dynamic Hysteresis Model Based on Vector-Play Model for Iron Loss Calculation Taking the Rotating Magnetic Fields Into Account,” *IEEE Trans. Mag.*, vol. 54, n° 3, pp. 1 – 4, 2018.

[51] S. Steentjes, D. Eggers, K. Hameyer, “Application and Verification of a Dynamic Vector-Hysteresis Model,” *IEEE Trans. Mag.*, vol. 48, n° 11, pp. 3379 – 3382, 2012.

[52] H. Yoon, M. Song, I. Kim, P. S. Shin, C. S. Koh, “Accuracy Improved Dynamic E&S Vector Hysteresis Model and its Application to Analysis of Iron Loss Distribution in a Three-Phase Induction Motor,” *IEEE Trans. Mag.*, vol. 48, n° 2, pp. 887 – 890, 2012.

[53] F.C. Meral, T.J. Royston, R. Magin, “Fractional calculus in viscoelasticity: An experimental study,” *Commun. Nonlinear Sci. Numer. Simulat.*, vol. 15, pp. 939 – 945, 2010.